Affine Neural Network Based Predictive Control Applied to a Distributed Solar Collector Field

Paulo Gil, *Member, IEEE*, Jorge Henriques, Alberto Cardoso, Paulo Carvalho, and António Dourado, *Member, IEEE*

***Abstract*—This paper presents experimental results concerning the control of a distributed solar collector field, where the main objective concerns the regulation of the outlet oil temperature by suitably manipulating the oil flow rate. This is achieved by means of a constrained nonlinear adaptive model-based predictive control framework where the control action sequence is obtained by solving an open loop optimization problem, subject to a set of constraints. The plant dynamics is approximated by an affine state-space neural network, whose complexity is specified in terms of the cardinality of dominant singular values associated with a subspace oblique projection of data driven Hankel matrices. The neural network is first trained offline and subsequently improved through a recursive updating of its weights and biases, based on a dual unscented Kalman filter. The control scheme was implemented on the Acurex field of the Plataforma Solar de Almería, Spain. Results from these experiments demonstrate the feasibility of the proposed framework, and highlighted the ability to cope with time-varying and unmodelled dynamics, under the form of disturbances, and its inherent capability for accommodating actuation faults.**

***Index Terms*—Model-based predictive control, adaptive control, constrained optimization, affine state-space neural networks, online training, unscented Kalman filter, distributed solar collector field.**

I. Introduction

THE modern societies way of life has been propped up on a high pace of fossil energy consumption *per capita*, which was constantly growing over the last century [1]. Inevitably, this behaviour is prompting a depletion of fossil energy reserves that is accompanied by an increase of air pollution, along with other forms of environmental degradation [2]. In order to mitigate such impacts on the environment, without compromising economic growth, it is crucial to implement a world-wide paradigm shift towards a non-carbon based economy. It implies not only energy conservation, but also the increase of renewable energy sources mix, such as, wind, hydroelectric or solar energy, which currently counts for less than 10 %, at world scale[1].

In the case of thermal solar power for electricity generation, there are some commercial systems in operation, most based on parabolic trough solar collectors, namely, the Andasol I & II in the Plateau of Guadix, Granada, Spain and the Solar Energy Generating Systems, in the Mojave Desert, California, USA (see e.g. [3] and references therein).

Parabolic trough solar systems concentrate irradiation on a linear absorber tube located at the focal line, while a heat transfer fluid, typically a synthetic oil, flows along the receiver pipes. In order to maximize the collected energy, regardless of possible disturbances acting on the system, namely, changes on direct solar radiation due to cloud cover, inlet oil temperature drift, or optical efficiency degradation, due to dirt deposition on the mirrors' surface, it is crucial that the control system should be designed in terms of favouring the closed loop performance and robustness alike [4].

Among advanced control techniques applied to distributed solar collector fields (DSC) to control the outlet heating fluid's temperature (see e.g. [5]) model-based predictive control (MPC) techniques have a number of appealing features, namely, providing optimal or suboptimal sequences of control actions, the potential for dealing with both input and output constraints, and the inherent ability for designing robust constrained control systems.

Different predictive control schemes have been applied to DSC systems (see e.g. [6]–[8]). Essentially, they all consider an explicit dynamic model of the plant within an optimisation thread in order to come up with an optimised sequence of control actions. In addition, most of the implementations also include a feedforward compensator in the control system to cope with measurable disturbances [6]. Although few implementation based on fixed parameters can be found in the literature, mainly because of the inherent nonlinear time-varying plant dynamics, it is worth mentioning the work of Camacho [9] where a generalized predictive controller was implemented on the Acurex field of the Plataforma Solar de Almería (PSA). In Camacho and Berenguel [6] an adaptive robust predictive control scheme was derived based on a simplified transfer function of the plant, considering the poles location fixed and zeros robustly identified online. According to the authors this control scheme showed poor performance in terms of static error, in the case of radiation and inlet oil temperature disturbances. Coito et al. [8] and Silva et al. [10] implemented a self-tuning control by multistep horizons (MUSMAR) framework on the Acurex field, while in [11] the authors propose a MUSMAR variant based on a bi-criteria optimization in order to improve the control system's performance in start-up transients. Experimental results have demonstrated the feasibility of these receding horizon ap-

P. Gil is with the Departmento de Engenharia Electrotécnica, Faculdade de Ciências e Tecnologia, Universidade Nova de Lisboa, Caparica, 2829-516, Portugal, e-mail: psg@fct.unl.pt, and with Centre for Informatics and Systems of the University of Coimbra (CISUC), University of Coimbra, Polo II, 3030-290, Coimbra, Portugal.

J. Henriques, A. Cardoso, P. Carvalho and A. Dourado are with CISUC, Informatics Engineering Department, University of Coimbra, Polo II, 3030-290, Coimbra, Portugal.

Manuscript received on July 19, 2012

[1] http://ourenergyfutures.org.

proaches. In Pickhardt and Silva [12] a nonlinear predictive control scheme is proposed assuming an input-output model of the plant within a receding horizon framework. The model's parameters are updated online at every sampling time to allow accommodating time-varying effects and modelling errors. Although the obtained results were promising, they show a significant underperformance of the control system in the presence of mild to severe radiation disturbances. In addition, as the authors stress, the underlying control law cannot incorporate an integral effect and the computation overhead in the optimization stage is quite dependent on the prediction horizon, which may have a direct impact on the sampling frequency.

A drawback of considering true nonlinear model-based predictive control (NMPC) techniques is linked to the need of solving a non-convex optimisation problem. Specifically, the convergence to a feasible/optimal solution and stability conditions cannot be guaranteed in advance, and the underlying computation time might exceed, by far, the specified sampling period. Moreover, in many cases, finding a good analytical model of the plant might be a very demanding, time consuming and costly task. As such, system identification should be favoured against analytical modelling, based on phenomenological considerations. An example of nonlinear black box structures are the artificial neural networks, which are quite appealing in terms of approximation and generalisation capabilities (see e.g. [13]–[17].

The above discussion motivates the development of a generic conceptual platform for nonlinear control system design, relying on a model-based predictive control framework, with the model of the plant described by an affine state-space three-layered neural network. The number of neurons to be included in the hidden layer is selected taking into account the specificity of the model structure and by applying the singular value decomposition (SVD) to a given oblique subspace projection. In order to cope with time-varying dynamics and modelling errors, an indirect adaptive scheme is suggested, where the neural network weights are updated by a recursive updating technique based on a dual unscented Kalman filter (DUKF) [18]. Finally, it should be mentioned that any comparisons, either in terms of performance or complexity, against other control techniques are out of scope in this work, being the reader referred to [4] and [5], and references therein, for a comprehensive discussion on control schemes applied to distributed solar collector fields.

The remainder of this paper is organized as follows. Section II introduces the affine state-space neural network topology, and describes the approaches considered for managing its complexity and training methodologies. Section III formulates the generic model-based control (MPC) scheme. In Section IV the distributed solar collector field (Acurex) of the Plataforma Solar de Almería, Spain, is described, while in Section V some experimental results are presented and discussed. Finally, Section VI concludes the paper.

II. Affine State-Space Neural Networks

Modelling nonlinear dynamic systems has been the main driving force for developing robust black-box topologies (see e.g. [19], [20]) in order to deal with unknown dynamics, nonlinearities and uncertainties. In this context, the ability of neural networks to learn based on input-output data and generalize to unseen data are quite appealing, in particular when the process dynamics is highly complex. In addition, their intrinsic approximation capabilities, scalability and inherent structural flexibility to cope with a larger class of problems are invaluable characteristics.

In the case of three-layered feedforward neural networks (input layer - hidden layer - output layer) consisting of sufficient number of hidden-layer's neurons with sigmoidal activation function, they can, in theory, approximate, to any level of accuracy, a given continuous nonlinear function (see e.g. [21]–[24]). However, this neural network topology is static by nature and consequently cannot inherently approximate spatio-temporal information. The way these structures can be used to emulate nonlinear systems' dynamics is typically carried out by providing the network with a regressor vector comprising past inputs and past outputs, being these structures dubbed as NARX (Nonlinear AutoRegressive with eXogenous inputs) neural networks.

Although NARX neural networks are effective in emulating nonlinear systems' dynamics (see e.g. [25]) they have some inescapable drawbacks. Specifically, they can only encode a finite number of previous inputs and outputs, they suffer from high sensitivity to the regressor's lag windows, and show a notorious susceptibility to noisy data.

A conceptually different way to represent nonlinear system dynamics is by incorporating feedback connections within the hidden layer of a three-layered neural network, where the remaining two layers are represented by the input layer and output layer. This architecture, referred to as state-space neural network, represents a broader class of nonlinear dynamic systems, and not only is less vulnerable to noisy data, but also the whole system history can inherently be embedded into the model. Moreover, state-space neural networks provide universal identification models in the restricted sense that they can approximate uniformly any multi input - multi output nonlinear dynamics over a finite time horizon, for every continuous and bounded input signal (see e.g. [26]).

A. Neural network architecture

The affine discrete-time state-space neural network topology considered in this work consists of three layers, as depicted in Fig. 1. The input layer and the output layer have as many neurons as the number of exogenous inputs and outputs of the dynamic system to be modeled, while the number of neurons to be incorporated within the hidden layer should be judiciously selected for the sake of generalization performance. A neural network comprising a deficient number of hidden layer neurons may not be feasible to appropriately emulate the underlying system dynamics, while a number of neurons larger than theoretically required may result in limited generalization performance due to overfitting. This problem is addressed in Section II-B.

The activation functions of neurons included in the hidden layer are both linear and sigmoidal, since in conjunction they

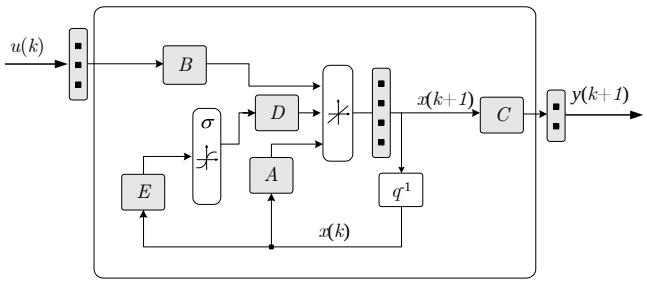

Fig. 1. Affine state-space neural network.

improve the neural predictor performance in case of mild nonlinear dynamics [27], and contribute to a less demanding training phase.

In state-space form the corresponding analytical model can be written as,

$$\begin{aligned} x\left(k+1\right) &= A\,x\left(k\right) + B\,u\left(k\right) + D\,\sigma\left(E\,x\left(k\right)\right) \\ y\left(k\right) &= C\,x\left(k\right) \end{aligned} \tag{1}$$

where $x \in \mathbb{R}^n$ denotes the hyperstate space vector, $y \in \mathbb{R}^p$ the output vector and $u \in \mathbb{R}^m$ the input vector. Matrices A, B, C, D and E are real-valued matrices of appropriate dimensions, while the nonlinear activation function $\sigma(\cdot)$ is a continuous and differentiable sigmoidal function, upper and lower bounded, satisfying the following conditions [28]:

- $\lim_{t\to\pm\infty}\sigma\left(t\right) = \pm 1$;
- $\sigma\left(t\right) = 0 \Leftarrow t = 0$;
- $\sigma'\left(t\right) > 0$;
- $\lim_{t\to\pm\infty}\sigma'\left(t\right) = 0$;
- $\max\left(\sigma'\left(t\right)\right) \leq 1 \Leftarrow t = 0$.

The reader is referred to [29] for a comprehensive survey on activation functions in artificial neural networks and [30] to a thorough study on stability conditions applied to the affine state-space architecture considered in this work.

B. Neural network complexity

This section deals with the problem of selecting an effective number of hidden layer neurons for the system represented in Fig. 1. Formally, it can be tackled by estimating an effective order for the affine state-space model (Eq. 1), assuming a linear approximation to the system's dynamics [31].

Let us assume a generic finite dimensional discrete-time invariant linear system represented in state-space form as,

$$\begin{aligned} x\left(k+1\right) &= A\,x\left(k\right) + B\,u\left(k\right) + \eta\left(k\right) \\ y\left(k\right) &= C\,x\left(k\right) + D\,u\left(k\right) + \vartheta\left(k\right) \end{aligned} \tag{2}$$

where $x \in \mathbb{R}^n$, $y \in \mathbb{R}^p$, $u \in \mathbb{R}^m$, $A \in \mathbb{R}^{n\times n}$, $B \in \mathbb{R}^{n\times m}$, $C \in \mathbb{R}^{p\times n}$ and $D \in \mathbb{R}^{p\times m}$. Vectors $\vartheta \in \mathbb{R}^p$ and $\eta \in \mathbb{R}^n$ are, respectively, unobserved Gaussian distributed, zero mean, white noise sequences accounting for the measurement noise and process noise. Additionally, suppose that the available data collected from the plant are ergodic and go to infinity, and Eq. (2) satisfies the orthogonality property, that is,

$$\mathcal{E}\left[\begin{pmatrix} x\left(k\right) \\ u\left(k\right) \end{pmatrix}\begin{pmatrix} \eta^T\left(k\right) & \vartheta^T\left(k\right) \end{pmatrix}\right] = 0 \tag{3}$$

with $\mathcal{E}$ denoting the expectation.

Consider now the past and future input block Hankel matrices, respectively, $U_p \equiv U_{0|i-1}$ and $U_f \equiv U_{i|2i-1}$ given by:

$$U_p = \begin{bmatrix} u\left(0\right) & u\left(1\right) & \cdots & u\left(j-1\right) \\ u\left(1\right) & u\left(2\right) & \cdots & u\left(j\right) \\ \vdots & \vdots & \ddots & \vdots \\ u\left(i-1\right) & u\left(i\right) & \cdots & u\left(i+j-2\right) \end{bmatrix} \tag{4}$$

$$U_f = \begin{bmatrix} u\left(i\right) & u\left(i+1\right) & \cdots & u\left(i+j-1\right) \\ u\left(i+1\right) & u\left(i+2\right) & \cdots & u\left(i+j\right) \\ \vdots & \vdots & \ddots & \vdots \\ u\left(2i-1\right) & u\left(2i\right) & \cdots & u\left(2i+j-2\right) \end{bmatrix} \tag{5}$$

and the past and future output block Hankel matrices, $Y_p \equiv Y_{0|i-1}$ and $Y_f \equiv Y_{i|2i-1}$ given according to,

$$Y_p = \begin{bmatrix} y\left(0\right) & y\left(1\right) & \cdots & y\left(j-1\right) \\ y\left(1\right) & y\left(2\right) & \cdots & y\left(j\right) \\ \vdots & \vdots & \ddots & \vdots \\ y\left(i-1\right) & y\left(i\right) & \cdots & y\left(i+j-2\right) \end{bmatrix} \tag{6}$$

$$Y_f = \begin{bmatrix} y\left(i\right) & y\left(i+1\right) & \cdots & y\left(i+j-1\right) \\ y\left(i+1\right) & y\left(i+2\right) & \cdots & y\left(i+j\right) \\ \vdots & \vdots & \ddots & \vdots \\ y\left(2i-1\right) & y\left(2i\right) & \cdots & y\left(2i+j-2\right) \end{bmatrix} \tag{7}$$

where the number of block rows i should be selected larger than the expected maximum order of the system under identification, that is, $n \ll i$ and the number of block columns $j \to \infty$.

The effective order for the linear model (2), which depends on the information embedded in the data set, can be retrieved from the rank of a subspace projection Π involving the above Hankel matrices (see e.g. [32].)

Definition 1 (Oblique projection)**.** *The oblique projection of the row space of $P \in \mathbb{R}^{p\times j}$ along the row space of $\Upsilon \in \mathbb{R}^{q\times j}$ on the row space of $\Gamma \in \mathbb{R}^{l\times j}$ is given by:*

$$P/_{\Upsilon}\Gamma = P\begin{bmatrix}\Gamma^T & \Upsilon^T\end{bmatrix}\left[\begin{pmatrix}\Gamma\Gamma^T & \Gamma\Upsilon^T \\ \Upsilon\Gamma^T & \Upsilon\Upsilon^T\end{pmatrix}^{\dagger}\right]_{1:l}\Gamma \tag{8}$$

with $\mathcal{M}^{\dagger}$ denoting the Moore-Penrose pseudoinverse of matrix $\mathcal{M}$.

Theorem 1 (Main subspace identification theorem [33])**.** *Under the assumptions that: a) the deterministic input is uncorrelated with the process noise η and measurement noise ϑ; b) the process noise η and the measurement noise ϑ are not identically zero; c) the exogenous input sequence is persistently exciting* [34] *of order $2\,i$; d) the data set is large ($j \to \infty$), then:*

1) *The projection Π_i can be defined as the oblique projection of the row space of Y_f on the past input/output row space along the row space of U_f,*

$$\Pi_i = Y_f /_{U_f} \begin{pmatrix} U_p \\ Y_p \end{pmatrix} \tag{9}$$

2) *The order of the linear discrete-time system is given by the number of non-zero singular values of Π_i.*

The number of non-zero singular values of Π_i reveals whether this projection is of full rank or rank deficient. In order to obtain the rank of Π_i the singular value decomposition (SVD) can be applied to the above projection, under the strict conditions of Theorem 1. Since the SVD provides orthonormal bases for range and null spaces, the cardinality of the column space of Π_i provides an estimate to the order of the linear system (2).

When this approach is applied to finite data sets ($j \ll \infty$) or in the case of data collected from nonlinear systems, even for large data sets exempt from coloured noise, the oblique projection matrix Π_i is full rank, that is, $\operatorname{rank}(\Pi_i) = i \cdot p$, irrespective of the number of row blocks i of the corresponding block Hankel matrices. In such cases it is imperative to reduce the column space of Π_i, by taking into account, for instance, the dominant singular values cardinality.

In the MATLAB© System Identification Toolbox [35] the implemented approach to estimate the system's order r searches for a gap in the singular values, being the order given by the largest integer, so that the corresponding singular value is greater than the geometric mean of the largest singular value σ_1 and the smallest non-zero singular value σ_s, that is,

$$r = \max\left\{ r : \log \sigma_r > \frac{1}{2}\left(\log \sigma_1 + \log \sigma_s\right) \right\} \tag{10}$$

A similar approach based on the search for a gap is presented in [36], where the estimate model order is given by,

$$r = \max\left\{ r : \frac{\sigma_r}{\sigma_{r+1}} > \frac{\sigma_\ell}{\sigma_{\ell+1}}, \forall\, \ell = 1, \ldots, s \wedge \ell \neq r \right\} \tag{11}$$

C. Training

The affine state-space neural network training is first carried out offline by using the Levenberg-Marquardt algorithm (see e.g. [37]), in particular because of its efficiency when the network contains no more than a few hundred parameters [38]. In the case of indirect adaptive MPC schemes this set of parameters is subsequently updated online by means of a recursive approach based on a dual Kalman filter. Its implementation relies, essentially, on the propagation of means and covariances through nonlinear transformations, referred to as *unscented transformation* (see e.g. [18], [39]). In the dual unscented Kalman filter framework both states and parameters are computed simultaneously in two different stages: *i*) the time update stage concerns the evaluation of one step-ahead predictions for states and parameters, while *ii*) in the measurement update a correction is made to these estimates on the basis of current noisy measurements.

Assume the general state-space nonlinear system written as:

$$\begin{aligned} x(k+1) &= f\left(x(k), u(k), w^f(k), k\right) + \eta(k) \\ z(k) &= g\left(x(k), u(k), w^g(k), k\right) + \vartheta(k) \end{aligned} \tag{12}$$

where $x \in \mathbb{R}^n$, $u \in \mathbb{R}^m$, $z \in \mathbb{R}^p$; $f(\cdot)$ and $g(\cdot)$ are real vector nonlinear functions with parametrisations w^f and w^g; $\eta \in \mathbb{R}^n$ and $\vartheta \in \mathbb{R}^p$ are random variables representing the process noise and measurement noise, respectively.

Taking into account the nonlinear black-box structure described by Eq. (12) the corresponding DUKF equations are as follows:

Weights estimation

Time update:

$$\Omega_i(k|k-1) = \Omega_i(k-1|k-1) \tag{13}$$

$$P_w(k|k-1) = P_w(k-1|k-1) + \Psi \tag{14}$$

$$\begin{aligned} Z_i^w(k|k-1) = g\big(&\hat{x}(k-1|k-1), u(k-1|k-1) \\ &, \Omega_i(k|k-1), k\big) \end{aligned} \tag{15}$$

$$\hat{z}_w(k|k-1) = \sum_{l=0}^{2N_w} \Gamma_l^w Z_l^w(k|k-1) \tag{16}$$

$$\begin{aligned} P_z^w(k|k-1) = \sum_{l=0}^{2N_w} \Big\{ &\Gamma_l^w \left[Z_l^w(k|k-1) - \hat{z}_w(k|k-1)\right] \\ &\cdot \left[Z_l^w(k|k-1) - \hat{z}_w(k|k-1)\right]^T \Big\} + \Upsilon \end{aligned} \tag{17}$$

$$\begin{aligned} P_{wz}(k|k-1) = \sum_{l=0}^{2N_w} \Big\{ &\Gamma_l^w \left[\Omega_l(k|k-1) - \hat{w}(k|k-1)\right] \\ &\cdot \left[Z_l^w(k|k-1) - \hat{z}_w(k|k-1)\right]^T \Big\} \end{aligned} \tag{18}$$

Measurement update:

$$K^w(k) = P_{wz}(k|k-1)\left[P_z^w(k|k-1)\right]^{-1} \tag{19}$$

$$\hat{w}(k|k) = \hat{w}(k|k-1) + K^w(k)\left[z(k) - \hat{z}_w(k|k-1)\right] \tag{20}$$

$$\begin{aligned} P_w(k|k) = &P_w(k|k-1) - K^w(k) P_z^w(k|k-1) \\ &\cdot \left(K^w(k)\right)^T \end{aligned} \tag{21}$$

with Ω the sigma points matrices of the vectorized affine state-space neural network weights $w = \left(w^f | w^g\right)$, P_w, P_z^w and P_{wz} covariance matrices, Z^w the observation matrix, $\hat{z}_w$ the weighted observation vector; Γ is the vector of weighting coefficients, K the Kalman gain; Υ denotes the measurement noise variance and Ψ the process noise.

State vector estimation

Time update:

$$\begin{aligned} \chi_l(k|k-1) = f\big(&\chi_l(k-1|k-1), u(k-1) \\ &\hat{w}(k-1|k-1), k\big) \end{aligned} \tag{22}$$

$$\hat{x}(k|k-1) = \sum_{l=0}^{2N_x} \Gamma_l^x \cdot \chi_l(k|k-1) \tag{23}$$

$$P_x\left(k|k-1\right)=\sum_{l=0}^{2N_x}\left\{\Gamma_l^x\left[\chi_l\left(k|k-1\right)-\hat{x}\left(k|k-1\right)\right]\cdot\left[\chi_l\left(k|k-1\right)-\hat{x}\left(k|k-1\right)\right]\right\}+\Theta \tag{24}$$

$$Z_i^x\left(k|k-1\right)=g\left(\chi_l\left(k-1|k-1\right),u\left(k-1|k-1\right),\hat{w}\left(k|k-1\right),k\right) \tag{25}$$

$$\hat{z}_x\left(k|k-1\right)=\sum_{l=0}^{2N_x}\Gamma_l^x Z_l^x\left(k|k-1\right) \tag{26}$$

$$P_z^x\left(k|k-1\right)=\sum_{l=0}^{2N_x}\left\{\Gamma_l^x\left[Z_l^x\left(k|k-1\right)-\hat{z}_x\left(k|k-1\right)\right]\cdot\left[Z_l^x\left(k|k-1\right)-\hat{z}_x\left(k|k-1\right)\right]^T\right\}+\Upsilon \tag{27}$$

$$P_{xz}\left(k|k-1\right)=\sum_{l=0}^{2N_x}\left\{\Gamma_l^x\left[\chi_l\left(k|k-1\right)-\hat{x}\left(k|k-1\right)\right]\cdot\left[Z_l^x\left(k|k-1\right)-\hat{z}_x\left(k|k-1\right)\right]^T\right\} \tag{28}$$

Measurement update:

$$K^x\left(k\right)=P_{xz}\left(k|k-1\right)\left[P_z^x\left(k|k-1\right)\right]^{-1} \tag{29}$$

$$\hat{x}\left(k|k\right)=\hat{x}\left(k|k-1\right)+K^x\left(k\right)\left[z\left(k\right)-\hat{z}_x\left(k|k-1\right)\right] \tag{30}$$

$$P_x\left(k|k\right)=P_x\left(k|k-1\right)-K^x\left(k\right)P_z^x\left(k|k-1\right)\cdot\left(K^x\left(k\right)\right)^T \tag{31}$$

where Θ is the process noise variance matrix and χ the sigma points matrices associated with the hyperstate vector x.

III. Model-Based Predictive Control

Model-based predictive control is a discrete-time technique where an explicit dynamic model of the plant is used to predict the system outputs over a finite horizon P, while a sequence of control actions is adjusted during a finite control horizon M in order to minimize a given cost function (see e.g. [40]). At time step k the optimiser computes online an optimal open loop sequence of control actions, so that the predicted outputs follow a pre-specified reference signal and taking into account possible hard and soft constraints. Only the current control action $u(k|k)$ is actually fed to the plant over the time interval $[k, k+1)$. Next, at time step $k+1$, the prediction and control horizons are shifted ahead by one step and a new open loop optimisation problem is solved using the most recent measurements from the plant and the control action fed to the plant at previous discrete-time $u(k|k)$.

Since the nonlinear model-based predictive control scheme developed in this work considers a local linear model of the plant derived at each discrete-time from the linearisation of the affine state-space neural network (Fig. 1), the remaining of this section will focus exclusively on the formulation of the constrained MPC tracking problem under the quadratic programming format.

Let the local linear discrete-time dynamic system be described in the state-space form as follows:

$$\begin{aligned}x\left(k+1\right)&=A\,x\left(k\right)+B\,u\left(k\right)\\y\left(k\right)&=C\,x\left(k\right)\end{aligned} \tag{32}$$

with $x\in\mathbb{R}^n$, $y\in\mathbb{R}^p$, $u\in\mathbb{R}^m$, $A\in\mathbb{R}^{n\times n}$, $B\in\mathbb{R}^{n\times m}$ and $C\in\mathbb{R}^{p\times n}$. In addition, assume that the performance index is defined as 2-norm and consider a set of linear constraints imposed on the system's inputs and outputs, along with a bound on the rate of change of the control action vector. Under the above premisses the open loop optimization problem can be stated as follows:

$$\Delta\mathcal{U}^*=\arg\min_{\Delta\mathcal{U}}\left\{\sum_{l=1}^{P}\left\|y\left(k+l|k\right)-r\left(k+l\right)\right\|_{Q_l}^2+\sum_{l=1}^{P-1}\left\|u\left(k+l|k\right)\right\|_{R_l}^2+\sum_{l=1}^{M-1}\left\|\Delta u\left(k+l|k\right)\right\|_{S_l}^2\right\} \tag{33}$$

subject to the system dynamics (32) and to the following set of constraints:

$$\begin{aligned}y_{min}\le y\left(k+l|k\right)\le y_{max},\,l=1,\ldots,P,\,k\ge0\\u_{min}\le u\left(k+l|k\right)\le u_{max},\,l=1,\ldots,P-1,\,k\ge0\\\left|\Delta u\left(k+l|k\right)\right|\le\Delta u_{max},\,l=1,\ldots,M-1,\,k\ge0\\\Delta u\left(k+l|k\right)=0\,,l=M,\ldots,P-1,\,k\ge0\end{aligned} \tag{34}$$

with $Q_l\in\mathbb{R}^{p\times p}$, R_l, $S_l\in\mathbb{R}^{m\times p}$; $\Delta u\in\mathbb{R}^m$ is the control action increment, $r\in\mathbb{R}^p$ denotes the reference signal and $\Delta\mathcal{U}^*$ the extended optimal control action sequence.

Since the cost function is quadratic and the set of constraints is linear, then optimization problem is convex and its solution is unique. In this case, the constrained open loop optimal control problem can be restated as a quadratic programming (QP) problem, namely,

$$\begin{aligned}\Delta\mathcal{U}^*=\arg\min_{\Delta\mathcal{U}}&\left\{h^{\mathrm{T}}\Delta\mathcal{U}+\frac{1}{2}\Delta\mathcal{U}^{\mathrm{T}}\mathcal{H}\,\Delta\mathcal{U}\right\}\\s.t.\quad&\mathcal{G}\cdot\Delta\mathcal{U}\le d\end{aligned} \tag{35}$$

where $\mathcal{G}\in\mathbb{R}^{(4m\cdot M+2p\cdot P)\times m\cdot M}$, $d\in\mathbb{R}^{(4m\cdot M+2p\cdot P)}$ and $\Delta\mathcal{U}\in\mathbb{R}^{m\cdot M}$. The gradient $h\in\mathbb{R}^{m\cdot M}$ and the Hessian $\mathcal{H}\in\mathbb{R}^{m\cdot M\times m\cdot M}$ are given by:

$$\begin{aligned}h_j^T=2\Bigg\{&x^T\left(k|k\right)\left[\sum_{i=j-1}^{P-1}\left(CA^{i+1}\right)^T Q_{i+1}\sum_{q=0}^{i-j+1}CA^q\right]B\\&-\left[\sum_{i=j-1}^{P-1}r^T\left(i+1\right)Q_{i+1}\sum_{q=0}^{i-j+1}CA^q\right]B\\&+u^T\left(k-1|k-1\right)\sum_{i=0}^{P-1}R_i\Bigg\}\end{aligned} \tag{36}$$

$$\begin{aligned}H_{jj}^T=2\Bigg\{&B^T\sum_{i=0}^{P-j}\left[\sum_{q=0}^{i}\left(CA^q\right)^T Q_{i+1}\sum_{q=0}^{i}CA^q\right]B\\&+\sum_{i=j-1}^{P-1}R_i+S_{j-1}\Bigg\}\\&(j=1,\ldots,M)\end{aligned} \tag{37}$$

$$H_{jl}^T = 2\left\{B^T \sum_{i=j-1}^{P-1}\left[\sum_{q=0}^{i-j+1}\left(CA^q\right)^T Q_{i+1}\sum_{q=0}^{i-l+1} CA^q\right]B + \sum_{i=j-1}^{M-1} R_i\right\} \quad (j,l=1,\ldots,M; j\neq l) \tag{38}$$

Concerning the constraint inequation, it follows that $\mathcal{G}$ is a block matrix defined as:

$$\mathcal{G} = \begin{pmatrix}\mathcal{G}_1\\ \mathcal{G}_2\\ \mathcal{G}_3\\ \mathcal{G}_4\\ \mathcal{G}_5\\ \mathcal{G}_6\end{pmatrix} \tag{39}$$

with

$$\mathcal{G}_1 = -\mathcal{G}_2\begin{pmatrix}\mathcal{I}_m & 0_m & \cdots & 0_m & 0_m\\ 0_m & \mathcal{I}_m & 0_m & 0_m & 0_m\\ \vdots & \vdots & \vdots & \vdots & \vdots\\ 0_m & 0_m & 0_m & 0_m & \mathcal{I}_m\end{pmatrix} \tag{40}$$

$$\mathcal{G}_3 = -\mathcal{G}_4 = \begin{pmatrix}\mathcal{I}_m & 0_m & \cdots & 0_m & 0_m\\ \mathcal{I}_m & I_m & 0_m & 0_m & 0_m\\ \vdots & \vdots & \vdots & \vdots & \vdots\\ \mathcal{I}_m & \mathcal{I}_m & \mathcal{I}_m & \mathcal{I}_m & \mathcal{I}_m\end{pmatrix} \tag{41}$$

$$\mathcal{G}_5 = -\mathcal{G}_6 = \begin{pmatrix}\phi_{11} & 0_{p\times m} & \cdots & 0_{p\times m} & 0_{p\times m}\\ \phi_{21} & \phi_{22} & 0_{p\times m} & \cdots & 0_{p\times m}\\ \vdots & \vdots & \vdots & \vdots & \vdots\\ \phi_{M1} & \phi_{M2} & \phi_{M3} & \cdots & \phi_{MP}\\ \vdots & \vdots & \vdots & \vdots & \vdots\\ \phi_{P1} & \phi_{P2} & \phi_{P3} & \cdots & \phi_{PM}\end{pmatrix} \tag{42}$$

where ϕ_{ij} is given by:

$$\phi_{ij} = C\sum_{q=0}^{i-j} A^q\cdot B, i=1,\ldots,P; j=1,\ldots,M\wedge j\leq i \tag{43}$$

With respect to the column vector d it takes the following form:

$$d = \begin{pmatrix}d_1\\ d_2\\ d_3\\ d_4\\ d_5\\ d_6\end{pmatrix} \tag{44}$$

$$d_1 = d_2 = \begin{pmatrix}\Delta u_{\max}(k|k)\\ \Delta u_{\max}(k+1|k)\\ \vdots\\ \Delta u_{\max}(k+M-1|k)\end{pmatrix} \tag{45}$$

$$d_3 = \begin{pmatrix}u_{\max}(k+|k) - u(k-1|k-1)\\ u_{\max}(k+1|k) - u(k-1|k-1)\\ \vdots\\ u_{\max}(k+M|k) - u(k-1|k-1)\\ \vdots\\ u_{\max}(k+P-1|k) - u(k-1|k-1)\end{pmatrix} \tag{46}$$

$$d_4 = \begin{pmatrix}-u_{\min}(k+|k) + u(k-1|k-1)\\ -u_{\min}(k+1|k) + u(k-1|k-1)\\ \vdots\\ -u_{\min}(k+M|k) + u(k-1|k-1)\\ \vdots\\ -u_{\min}(k+P-1|k) + u(k-1|k-1)\end{pmatrix} \tag{47}$$

$$d_5 = \begin{pmatrix}c_1^{\bar{y}}\\ c_2^{\bar{y}}\\ \vdots\\ c_P^{\bar{y}}\end{pmatrix} \tag{48}$$

$$d_6 = \begin{pmatrix}c_1^{\underline{y}}\\ c_2^{\underline{y}}\\ \vdots\\ c_P^{\underline{y}}\end{pmatrix} \tag{49}$$

with

$$c_i^{\bar{y}} = y_{\max} - C\left[A^i x(k|k) + \sum_{j=0}^{i-1} A^j Bu(k-1|k-1)\right] \tag{50}$$

and

$$c_i^{\underline{y}} = -y_{\min} + C\left[A^i x(k|k) + \sum_{j=0}^{i-1} A^j Bu(k-1|k-1)\right] \tag{51}$$

where $y_{\max}$ denotes the maximum allowable output from the plant, and $y_{\min}$ corresponds to the admissible minimum output.

IV. Solar Power Plant Setup

A. Description

The distributed solar collector field (Acurex) used as a testbed for model-based predictive control experiments is owned by the Plataforma Solar de Almería (PSA), and is located in the desert of Tabernas, in the South of Spain. The Acurex plant is part of a small Solar Power System (SPS), which includes, in addition, a thermal storage tank system and a power unit (see Fig. 2).

The DSC field (Fig. 3) consists of 480 parabolic trough collectors arranged in 20 rows aligned on a West-East axis and forming 10 independent loops. Each solar collector is a linear parabolic-shaped reflector that focuses the sun's beam radiation on a linear absorber pipe located at the focus of the parabola. Each loop is 172 m long, with an active section of 142 m, while the reflective area of the mirrors is around 264.4 m^2.

The heat transfer fluid used to transport the thermal energy is the Santotherm 55, which is a synthetic oil with a maximum

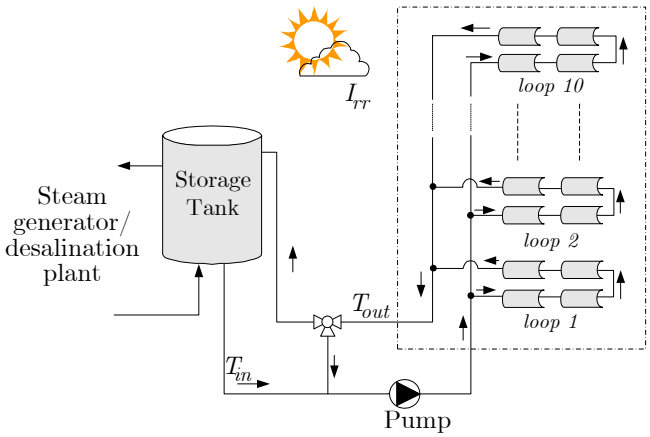

Fig. 2. PSA's Solar Power System schematics.

Fig. 3. Acurex solar collector loop.

film temperature of 318 °C and an autoignition temperature of 357 °C. The thermal oil is heated as it circulates through the absorber pipe before entering the top of the storage tank. The colder inlet oil is extracted form the bottom of the tank, while a three way valve located at the field outlet enables the oil recycling (by-passing the storage tank) until the outlet oil temperature is high enough to be sent to the tank. The thermal energy stored in the tank is subsequently used to generate electricity in a conventional steam turbine/generator or consumed in the solar desalination plant. The main reason for including a storage tank in the SPS is to provide a buffer between the electricity production and the solar energy availability.The DSC field is provided with a sun tracking system, which causes the solar collector to revolve around an axis parallel to the receiver in order to follow the yearly variation of the sun's declination.

The DSC field operating limits are, in terms of oil flow rate, restricted to a minimum of 2.0 l/s and a maximum of 12.0 l/s. The lower bound is imposed to reduce the risk of oil decomposition, which occurs when its temperature exceeds 305 °C, while the maximum bound is related to the admissible pressure drop along the pipe length.

From the control point of view, the main difference between a standard power plant and a thermal solar power plant is that the energy source (solar radiation) cannot be manipulated. Moreover, the direct solar radiation is seasonally dependent, varies throughout the day and is susceptible to atmospheric conditions, such as cloud cover, humidity and turbidity. In this context, the objective of the control system is to maintain the outlet oil temperature at a prescribed value irrespective of variations on the beam solar radiation, inlet oil temperature and solar collectors' reflectivity, while taking into account hard constraints imposed on the system, and by manipulating the oil flow rate through each loop.

B. Solar Collector Field Identification

Regarding the identification of the Acurex field for control purpose, the outlet oil temperature T_{out} (system output) depends not only on the oil flow rate Q_{in}(input), but also on other variables, such as the inlet oil temperature T_{in}, solar radiation I_{rr}, ambient temperature and mirrors reflectivity. Since the solar beam radiation and the inlet oil temperature are measurable, it is worth incorporating a feedforward compensator (Fig. 4) in series with the plant (see e.g. [4]).

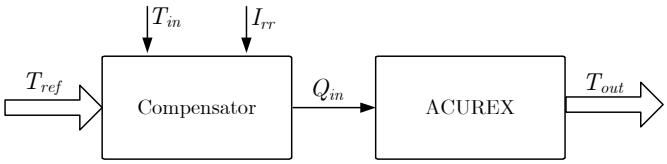

Fig. 4. Feedforward compensator.

This feedforward term is derived for steady state conditions and delivers the required oil flow rate demanded to the pump, provided the desired outlet oil temperature T_{ref}, solar beam radiation and inlet oil temperature are known. The feedforward term was implemented according to following general expression:

$$Q_{\text{in}} = \frac{\mu \cdot N_{\text{act}} \cdot I_{\text{c}} \cdot A_{\text{eff}}}{\rho \cdot c_p \left(T_{\text{ref}} - T_{\text{in}}\right)} \tag{52}$$

where μ is a coefficient to be computed experimentally, N_{act} the number of active loops, I_{c} the corrected solar radiation computed from the solar beam radiation I_{rr}, A_{eff} denotes the effective mirrors' surface of each loop, ρ is the oil specific mass and c_p is the specific thermal capacity.

The input to the feedforward compensator is the reference outlet oil temperature, while the corresponding output is associated with the oil flow rate, and the remaining variables,

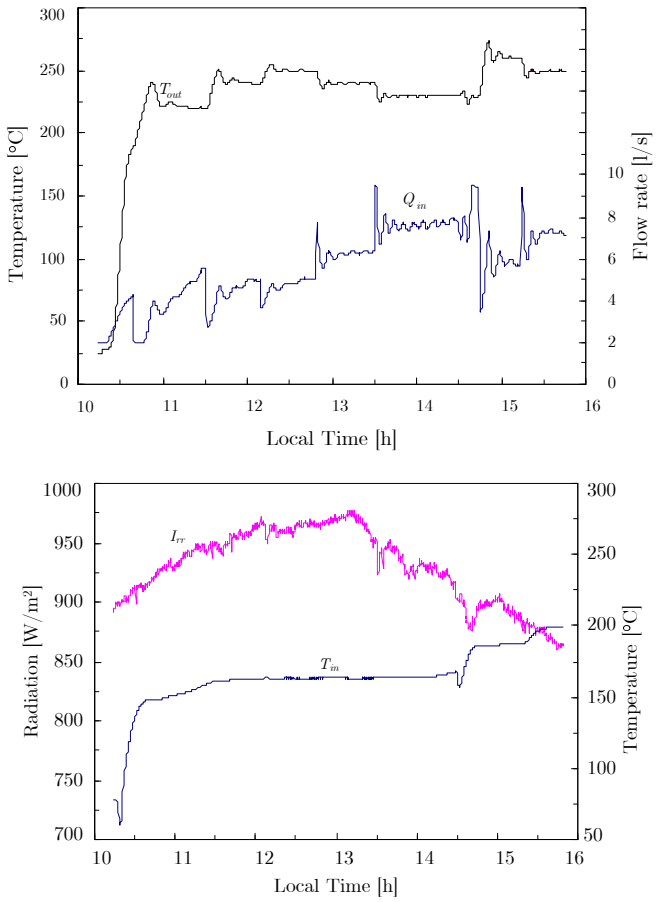

Fig. 5. Data set collected from the Acurex field.

namely, T_{in} and I_c, can be regarded as measurable disturbances acting on the pseudo-system.

For the Acurex identification two data sets have been collected from the plant to be used in the neural network training and validation phases. They included the outlet oil temperature (T_{out}), the inlet oil temperature (T_{in}), the flow rate (Q_{in}) and the solar beam radiation (I_{rr}), at a sample rate of 15 s. One of those data sets is plotted in Fig. 5. In order to come with an estimate for the effective order of the affine state-space neural network the approach proposed in Sec. II-B is then applied. Taking into account the data set presented in Fig. 5 and a number of row blocks chosen as $i = 20$, which is substantially higher than the expected effective dominant singular values cardinality, the singular values associated with the projection matrix Π_{20} are presented in (53). From the singular values inspection, in terms of absolute magnitude and magnitude decay, it is clear that the dominant vector basis is quite lower than the rank of Π_{20}. Hence, a post-processing procedure should be considered to reduce the model's complexity. It should be mentioned that, in the present case, full rankness is mainly due to nonlinear dynamics embedded in the data sets, and also to a finite data set ($j << \infty$) collected from the plant.

In order to reduce the vector basis dimension let us consider the methodology based on (10), that is,

$$r = \max\{r \,:\, \log\sigma_r > -0.1920\}$$

The largest integer satisfying the previous inequality is 6, which points to a 6^{th} order model to approximate the plant's dynamics embedded in the collected data and considering a linear approximation under the form of Eq. (2).

$$\sigma = \begin{pmatrix} 1381.623814 \\ 28.650875 \\ 27.872150 \\ 5.312726 \\ 1.814615 \\ 1.054868 \\ 0.719611 \\ 0.389758 \\ 0.387268 \\ 0.354688 \\ 0.293651 \\ 0.279058 \\ 0.262657 \\ 0.165907 \\ 0.138188 \\ 0.099948 \\ 0.099164 \\ 0.038363 \\ 0.031553 \\ 0.000493 \end{pmatrix} \tag{53}$$

To assess the 6^{th} order affine state-space model performance, the neural network was trained offline using the Levenberg-Marquardt algorithm, within the MATLAB© environment. Fig. 6 compares the outlet oil temperature collected on the Acurex field with the corresponding prediction provided by the affine state-space neural network. As can be observed, the neural predictor's output is in line with the distributed solar collector field behaviour, either in terms of overshoot, settling time and static gain. Nevertheless, a slight model-plant mismatch is still detected, which is confirmed by the Mean Normalized Absolute Error (MNAE) magnitude, namely, 1.10×10^{-2}. This fact suggests the need for an improvement in terms of generalization capabilities of the neural network approximator, by considering, for instance, a recursive-based updating approach.

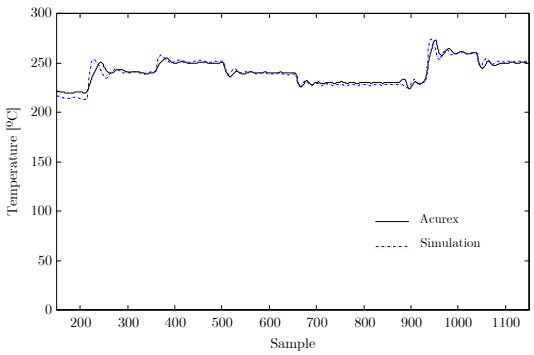

Fig. 6. Acurex outlet oil temperature versus neural network simulation.

V. Solar Collector Field Tests

The nonlinear MPC scheme was tested on the Acurex field of PSA in two different strategies, namely, indirect adaptive and non-adaptive. In either cases, for regulating or driving the outlet oil temperature to a pre-specified level, despite variations in the sun's beam radiation and in inlet oil temperature, the control system manipulates the thermal oil flow rate pumped to the solar collector field.

Given the computation complexity and memory requirements of this approach, it was chosen to run the main routines, namely, online identification, in the case of adaptive schemes, state estimation, and the open loop optimisation, on a remote computer, more specifically a laptop computer. This allowed to implement these routines in MATLAB© taking advantage of its programming flexibility and the available toolboxes, such as the optimisation toolbox, for solving the required open loop constrained quadratic optimisation problem.

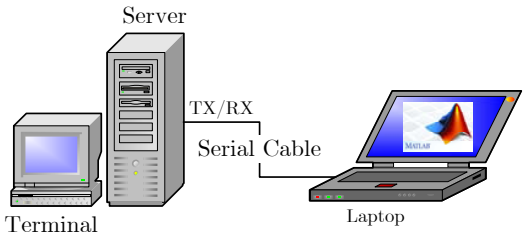

Fig. 7. Laptop-Server serial communication.

The laptop computer was connected with the Acurex field Server via RS232 serial communication (Fig. 7), which provides the physical means for the exchange of data. In this framework, the Acurex control server supplies the laptop with the DSC field data, which computes a new control action sequence under the form of oil flow rate. The new oil flow rate $u(k|k)$ is then sent to the laptop's COM and read by the Acurex field server. Next, the Server forwards the control action, regarded as a reference flow rate, to the pump PI (Proportional-Integral) controller. The communication routines for synchronisation, sending and reading have been implemented both in C code and included in the Acurex software package and also in MATLAB© to be called within the control cycle implemented on the remote laptop.

In all the experiments reported in this work it was considered a prediction horizon $P = 10$ time-steps, a control horizon $M = 1$ and the weight matrices associated with the performance index presented in (54). These penalty matrices were selected by a trial and error heuristic, using a simulation software package for the Acurex Solar collector field [41], and considering as design-based conditions the step response's overshoot and settling-time.

$$\begin{aligned} Q_i &= \begin{cases} 5, & i = 1, \ldots, P-1 \\ 100, & i = P \end{cases} \\ R_i &= 10^{-3}, \quad i = 1, \ldots, P-1 \\ S_i &= 10^{-4}, \quad i = 1, \ldots, M-1 \end{aligned} \tag{54}$$

In what the hard constraints included in the optimization problem are concerned, they reflect physical limitations of the Acurex field. The oil flow rate was set as lying within 2.0 l/s and 10.0 l/s, being the upper bound lower than the maximum admissible flow rate for safety reasons, while the outlet oil temperature is limited to 300 °C. In addition, the maximum oil flow rate increments were constrained to 0.1 l/s, in order to enable a smooth pump operation, which contributes to maximizing the main oil pump lifespan. In terms of sampling time, unlike the experiment reported in Section V-C, in which was considered a sampling time of 10 s, all the remaining experiments were conducted considering a sampling time of 15 s.

A. Non-Adaptive MPC

This experiment concerns an MPC control configuration in which the neural affine state-space neural network predictor is not updated in the course of the conducted tests, and the unscented Kalman filter is only used for state estimation .

The main purpose of this experiment is twofold: to evaluate the performance of a non-adaptive framework in controlling the Acurex field and to use it on comparison basis to assess improved MPC schemes performance, namely the indirect adaptive approach.

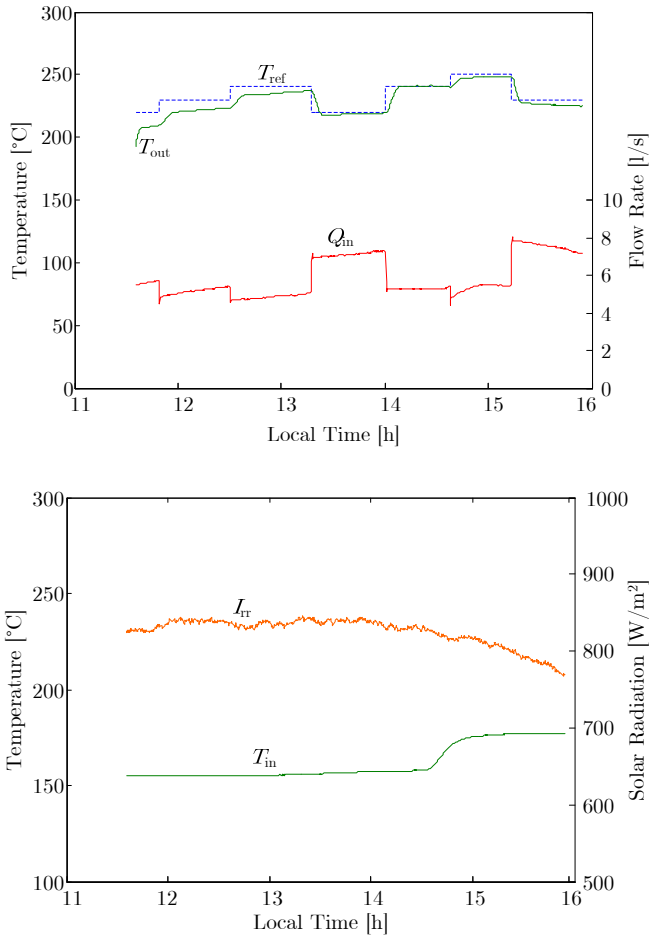

Fig. 8. Non-adaptive MPC.

In Fig. 8 are presented the outcomes of one of the experiments carried out at the site, for which the nonlinear model parameters are fixed, and assuming $P_x(0) = \mathcal{I}$, see Eq. (24). In this figure it is shown the outlet oil temperature (T_{out}), the oil reference temperature (T_{ref}), the control action ($u(k|k)$), under the form of demanded flow rate in each loop (Q_{in}), the oil inlet temperature (T_{in}) and the solar beam radiation prior to correction (I_{rr}), over time.

As can be observed from Fig. 8, the pump has a smooth operation, although a residual static offset is evident for some operating point, which is mainly attributed to model-plant mismatch. Moreover, the control system performance is not significantly affected by disturbances on solar beam radiation and inlet oil temperature, as they are accommodated by the feedforward compensator expressed in terms of Eq. (52).

B. Indirect Adaptive MPC

This Section considers the implementation of an indirect adaptive MPC scheme on the Acurex field, for which the plant parameters are adjusted online in order to cope with unmodelled dynamics and disturbances. A dual unscented Kalman filter, as proposed in Section II-C, was used for recursive parameter estimation and state estimation. Initial covariance matrices were chosen as $P_w(0) = 5.0 \times 10^{-3}\mathcal{I}$ and $P_x(0) = \mathcal{I}$. Additionally, a forgetting factor $\tau = 0.9986$ was also considered by rewriting Eq. (14) as:

$$P_w\left(k|k-1\right) = \frac{1}{\tau} P_w\left(k-1|k-1\right) \tag{55}$$

The Fig. 9 shows results of an experiment where the adaptive MPC scheme was incorporated in the control loop. From these results it is possible to infer that the control system is "well-behaved" despite disturbances on the solar beam radiation and inlet oil temperature. Furthermore, given the indirect adaptive trait of this controller, which relies on recursive nonlinear identification techniques, modelling errors are progressively attenuated, which benefits the steady-state control system behaviour, namely the static error, in comparison with non-adaptive schemes. Finally, a mention should be made to the fact that right after the control policy has been switched to the MPC, a rather prominent overshoot is noticed, along with slight oscillations in the outlet oil temperature, which can be explained in part by the adaptation mechanisms that are in play.

C. Indirect Adaptive MPC - Actuation Fault

This experiment intends to assess the control system behaviour and robustness for an operation fault on the actuation system. This fault was taking place on the variable speed drive attached to the main pump, and was imposing a difference in the pumped oil flow rate with respect to the reference oil flow rate provided by the MPC scheme. In the case of the experiment in question, the flow rate deviation given by the difference between the prescribed oil flow rate and the measured value *in loco* is presented in Fig. 10. As can be observed, most of the time the prescribed oil flow rate was

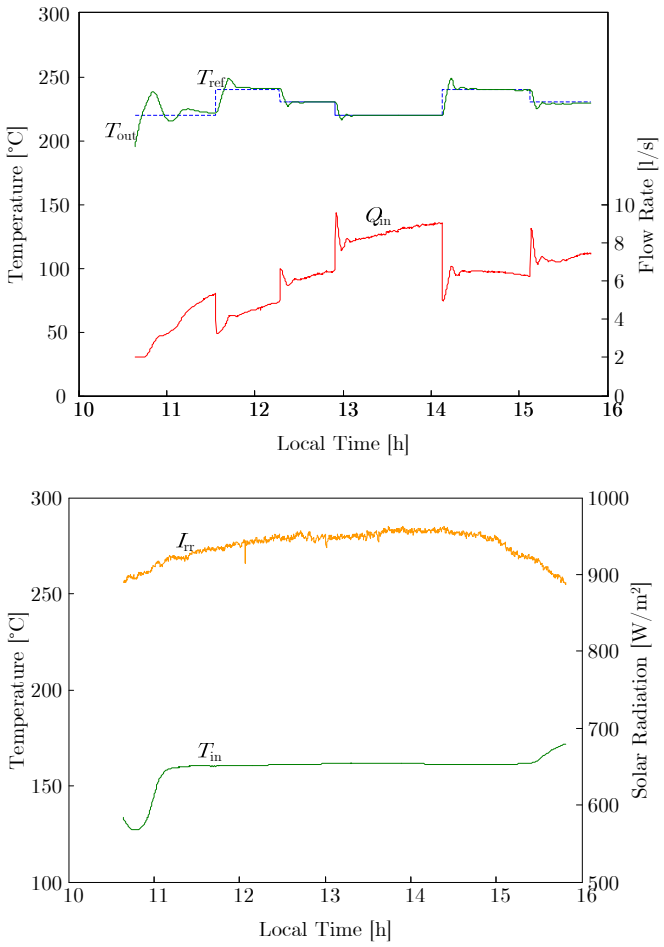

Fig. 9. Indirect adaptive MPC.

higher than that fed to the Acurex field. As a result, this will lead to a positive offset of the oil flow rate temperature if the corresponding effect is not appropriately accommodated by the control system.

The experiment was run using the indirect adaptive MPC scheme with a sampling time of 10 s, and considering the same covariance matrices as those presented in Sec. V-B, together with $\tau = 0.9987$. The obtained results are shown in Fig. 11.

As can be observed from this figure, the indirect adaptive MPC scheme is able to drive the outlet oil temperature to the corresponding reference, in spite of a malfunctioning pending on the variable speed drive. The accommodation of this fault is carried out by the joint contribution of online identification, which incorporates into the Acurex field dynamics the actuation fault, and the state estimation procedure.

In what the sampling time is concerned, no significant difference is detected in terms of performance by choosing more stringent admissible values for the sampling time. However, further studies have to be conducted on site to confirm this assertion.

VI. Conclusions

This paper presented the implementation of a constrained affine state-space neural network based predictive control

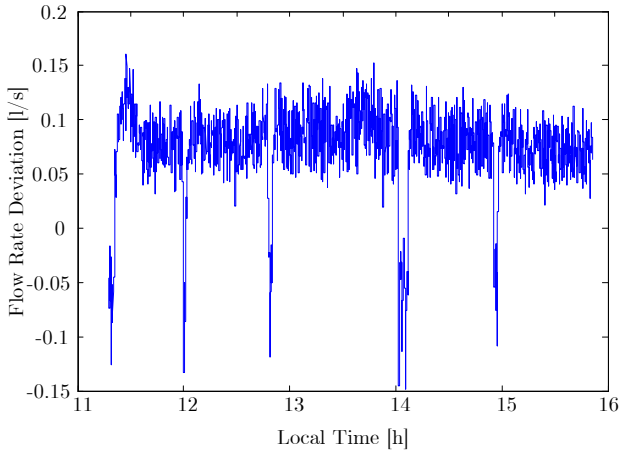

Fig. 10. Oil flow rate deviation.

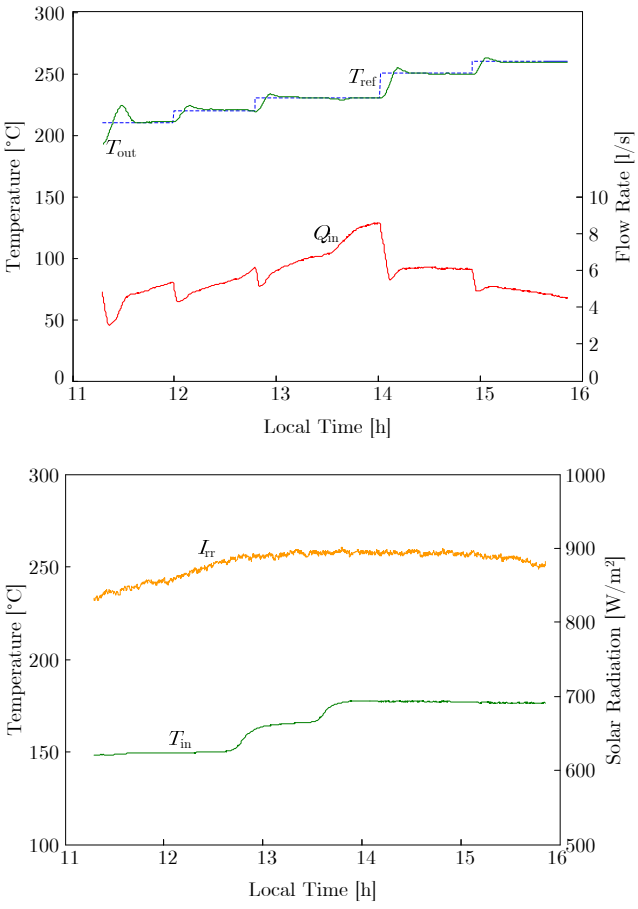

Fig. 11. Indirect adaptive MPC - actuation fault.

scheme on a distributed solar collector (Acurex) field, owned by the Plataforma Solar de Almería, where the main goal consists in driving the outlet oil temperature to a prescribed value. The neural network predictor's complexity measured by the order of the state-space nonlinear model, is dealt with by estimating the number of dominant singular values of a subspace oblique projection of data driven Hankel matrices. In order to guarantee that the optimization problem convexity is held, the dynamic model of the Acurex field, described by an affine state-space neural network, is locally linearised, while the optimisation problem constraints are represented by a set of linear inequalities. The online updating of the neural network weights and state estimation is based on a dual unscented Kalman filter. In the case of the non-adaptive MPC framework only a state estimation is carried out.

Experiments conducted on the Acurex field included tests based on a non-adaptive MPC scheme and on an indirect adaptive version. The first implementation showed that as a result of model-plant mismatch the outlet oil temperature displays a static offset, irrespective of the operating regime. This effect was practically removed in the indirect-adaptive formulation, due to a neural model improvement, which is gradually achieved by means of a recursive adjusting of weights, based on new data collected from the plant.

Concerning the MPC robustness to measurable disturbances, such as solar beam radiation and inlet oil temperature, they were effectively accommodated by the feedforward compensator as the experiments reveal. In addition, in the case of a faulty actuator, resulting from a malfunction on the variable speed drive that is attached to the main pump of the Acurex field, the indirect adaptive MPC framework was able to accommodate its impact on the outlet oil temperature.

Acknowledgment

The experiments included in this work have been carried out within the project Improving Human Potential Program (EC-DGXII), supported by the European Union Program Training and Mobility of Researchers. The authors would like to express their gratitude to the staff of the Plataforma Solar de Almería.

References

[1] K. Lei and S. Zhou, "Per capita resource consumption and resource carrying capacity: A comparison of the sustainability of 17 mainstream countries," *Energy Policy*, vol. 42, no. 0, pp. 603 – 612, 2012.

[2] S. V. A. R. Sastry and P. Sreenu, "New energy sources and its sustainability," in *Engineering Education: Innovative Practices and Future Trends (AICERA), 2012 IEEE International Conference on*, July 2012, pp. 1–15.

[3] G. Manzolini, M. Bellarmino, E. Macchi, and P. Silva, "Solar thermodynamic plants for cogenerative industrial applications in southern europe," *Renewable Energy*, vol. 36, no. 1, pp. 235 – 243, 2011.

[4] E. Camacho, F. Rubio, M. Berenguel, and L. Valenzuela, "A survey on control schemes for distributed solar collector fields. part I: Modeling and basic control approaches," *Solar Energy*, vol. 81, no. 10, pp. 1240 – 1251, 2007.

[5] ——, "A survey on control schemes for distributed solar collector fields. part II: Advanced control approaches," *Solar Energy*, vol. 81, no. 10, pp. 1252 – 1272, 2007.

[6] E. F. Camacho and M. Berenguel, "Robust adaptive model predictive control of a solar plant with bounded uncertainties," *International Journal of Adaptive Control and Signal Processing*, vol. 11, no. 4, pp. 311–325, 1997.

[7] C. Greco, G. Menga, E. Mosca, and G. Zappa, "Performance improvements of self-tuning controllers by multistep horizons: The musmar approach," *Automatica*, vol. 20, no. 5, pp. 681 – 699, 1984.

[8] F. Coito, J. M. Lemos, R. N. Silva, and E. Mosca, "Adaptive control of a solr energy plant: Exploiting accessible disturbances," *International Journal of Adaptive Control and Signal Processing*, vol. 11, no. 4, pp. 327–342, 1997.

[9] E. Camacho, *Advances in Model-Based Predictive Control*. Oxford University Press, 1994, ch. Application of GPC to a solar power plant.

[10] R. Silva, L. Rato, J. Lemos, and F. Coito, "Cascade control of a distributed collector solar field," *Journal of Process Control*, vol. 7, no. 2, pp. 111 – 117, 1997.

[11] R. Silva, N. Filatov, J. Lemos, and H. Unbehauen, "Feedback/feedforward dual adaptive control of a solar collector field," in *Control Applications, 1998. Proceedings of the 1998 IEEE International Conference on*, vol. 1, Sep 1998, pp. 309 –313 vol.1.

[12] R. Pickhardt and R. Neves da Silva, "Application of a nonlinear predictive controller to a solar power plant," in *Control Applications, 1998. Proceedings of the 1998 IEEE International Conference on*, vol. 1, Sep 1998, pp. 6 –10 vol.1.

[13] K. Patan, "Stability analysis and the stabilization of a class of discrete-time dynamic neural networks," *Neural Networks, IEEE Transactions on*, vol. 18, no. 3, pp. 660 –673, May 2007.

[14] X. Han, W.-F. Xie, Z. Fu, and W. Luo, "Nonlinear systems identification using dynamic multi-time scale neural networks," *Neurocomputing*, vol. 74, no. 17, pp. 3428 – 3439, 2011.

[15] H. Wei, S. Billings, Y. Zhao, and L. Guo, "An adaptive wavelet neural network for spatio-temporal system identification," *Neural Networks*, vol. 23, no. 10, pp. 1286 – 1299, 2010.

[16] B. S. Leon, A. Y. Alanis, E. N. Sanchez, E. Ruiz-Velazquez, and F. Ornelas-Tellez, "Inverse optimal neural control for a class of discrete-time nonlinear positive systems," *International Journal of Adaptive Control and Signal Processing*, 2012.

[17] J. Henriques, P. Gil, P. Carvalho, H. Duarte-Ramos, and A. Dourado, *Power Plant Applications of Advanced Control Techniques*. ProcessEng Engineering GmbH, 2010, ch. Nonlinear Control Based on Affine Neural Networks: Applicatiion to a Solar Power Plant, pp. 295–320.

[18] S. Julier, J. Uhlmann, and H. Durrant-Whyte, "A new method for the nonlinear transformation of means and covariances in filters and estimators," *Automatic Control, IEEE Transactions on*, vol. 45, no. 3, pp. 477 –482, mar 2000.

[19] A. Juditsky, H. Hjalmarsson, A. Benveniste, B. Deylon, L. Ljung, J. Sjberg, and Q. Zhang, "Nonlinear black-box modeling in system identification: Mathematical foundations," *Automatica*, vol. 31, pp. 1725 – 1750, 1995.

[20] J. Sjberg, Q. Zhang, L. Ljung, A. Benveniste, B. Deylon, P. yves Glorennec, H. Hjalmarsson, and A. Juditsky, "Nonlinear black-box modeling in system identification: a unified overview," *Automatica*, vol. 31, pp. 1691–1724, 1995.

[21] G. Cybenko, "Approximation by superpositions of a sigmoidal function," *Math. Control, Signals Syst*, vol. 2, pp. 303–314, 1989.

[22] K. Funahashi, "On the approximate realization of continuous mappings by neural networks," *Neural Networks*, vol. 2, pp. 183–192, 1989.

[23] K. Hornik, M. Stinchcombe, and H. White, "Multilayer feedforward networks are universal approximators," *Neural Networks*, vol. 2, pp. 359–366, 1989.

[24] M. Leshno, V. Lin, A. Pinkus, and S. Schocken, "Multilayer feedforward networks with a nonpolynomial activation function can approximate any function," *Neural Networks*, vol. 6, no. 6, pp. 861–867, 1993.

[25] Siegelmann, Horne, and Giles, "Computational capabilities of recurrent NARX neural networks," *IEEETSMC: IEEE Transactions on Systems, Man, and Cybernetics*, vol. 27, no. 2, pp. 208–215, 1997.

[26] E. Sontag, "Recurrent neural networks: Some systems-theoretic aspects," in *Dealing with Complexity: a Neural Network Approach*. Springer-Verlag, 1997, pp. 1–12.

[27] D. T. Pham and X. Liu, *Neural Networks for Identification, Prediction and Control*. Springer, 1995.

[28] Q. Dong, K. Matsui, and X. Huang, "Existence and stability of periodic solutions for hopfield neural network equations with periodic input," *Nonlinear Analysis: Theory, Methods & Applications*, vol. 49, no. 4, p. 471 479, 2002.

[29] W. Duch and N. Jankowski, "Survey of neural transfer functions," *Neural Computing Surveys*, vol. 2, pp. 163–212, 1999.

[30] P. Gil, J. Henriques, A. Cardoso, and A. Dourado, "On affine state-space neural networks for system identification: Global stability conditions and complexity management," *Control Engineering Practice*, vol. 21, no. 4, pp. 518 – 529, 2013.

[31] P. Gil, J. Henriques, A. Dourado, and H. Duarte-Ramos, "Order estimation in affine state-space neural networks," in *Soft Computing in Industrial Applications, 2005. SMCia/05. Proceedings of the 2005 IEEE Mid-Summer Workshop on*, June 2005, pp. 132 – 137.

[32] V. Sima, D. M. Sima, and S. V. Huffel, "High-performance numerical algorithms and software for subspace-based linear multivariable system identification," *Journal of Computational and Applied Mathematics*, vol. 170, no. 2, p. 371397, 2004.

[33] B. D. Moor, P. Overschee, and W. Favoreel, "Algorithms for subspace state-space identification: An overview," in *Applied and computational control, signals, and circuits*, B. N. Datta, Ed. Birkhuser, 1999, vol. 1, ch. 6, pp. 247 – 311.

[34] K. Åström, "Maximum likelihood and prediction error methods," *Automatica*, vol. 16, no. 5, p. 551574, 1980.

[35] L. Ljung, *System Identification Toolbox: Users's Guide*. The MathWorks, Inc., 1995.

[36] H. Yin, Z. Zhu, and F. Ding, "Model order determination using the hankel matrix of impulse responses," *Applied Mathematics Letters*, Jan. 2011.

[37] P. Gill and W. Murray, "Algorithms for the solution of the nonlinear least-squares problem," *SIAM Journal on Numerical Analysis*, vol. 15, no. 5, pp. 977–992, 1978.

[38] A. Suratgar, M. Tavakoli, and A. Hoseinabadi, "Modified levenberg-marquardt method for neural networks training," in *Proceedings - Wec 05: Fourth World Enformatika Conference*, 2005.

[39] E. Wan and R. Van Der Merwe, "The unscented kalman filter for nonlinear estimation," in *Adaptive Systems for Signal Processing, Communications, and Control Symposium 2000. AS-SPCC. The IEEE 2000*, 2000, pp. 153 –158.

[40] J. Maciejowski, *Predictive Control with Constraints*. Prentice Hall, 2002.

[41] M. Berenguel, E. Camacho, and F. Rubio, "Simulation software package for the acurex field," Departamento de Ingeniería de Sistemas y Automática, ESII, Universidad de Sevilla, Tech. Rep., 1994.